Nano Energy 43 (2018) 149–158

Contents lists available at ScienceDirect

Nano Energy

journal homepage: www.elsevier.com/locate/nanoen

Full paper

Interface engineering for high-performance direct methanol fuel cells using multiscale patterned membranes and guided metal cracked layers

Segeun Jang[a,b,1], Sungjun Kim[c,d,1], Sang Moon Kim[e], Jiwoo Choi[a,b], Jehyeon Yeon[a,b], Kijoon Bang[a,b], Chi-Yeong Ahn[c,d], Wonchan Hwang[c,d], Min Her[c,d], Yong-Hun Cho[f,*], Yung-Eun Sung[c,d,**], Mansoo Choi[a,b,***]

[a] Global Frontier Center for Multiscale Energy Systems, Seoul National University, Seoul 08826, Republic of Korea
[b] Department of Mechanical and Aerospace Engineering, Seoul National University, Seoul 08826, Republic of Korea
[c] Center for Nanoparticle Research, Institute for Basic Science (IBS), Seoul 08826, Republic of Korea
[d] School of Chemical and Biological Engineering, Seoul National University, Seoul 08826, Republic of Korea
[e] Department of Mechanical Engineering, Incheon National University, Incheon 22012, Republic of Korea
[f] Department of Chemical Engineering, Kangwon National University, Samcheok 24341, Republic of Korea

ARTICLE INFO

Keywords:
Creep behavior
Multiscale patterning
Crack
Direct methanol fuel cell
Methanol crossover
Membrane electrode assembly

ABSTRACT

Capability to fabricate high-performance membrane electrode assemblies (MEAs) is a key to the commercialization of direct methanol fuel cells (DMFCs). This work reports an interface engineering method to introduce a multiscale patterned membrane and a guided metal cracked layer between the catalyst layer and the membrane by the creep-assisted sequential imprinting and simple stretching technique. The MEA with a multiscale patterned membrane, where the nanopatterns covered the whole surface even on the side surface of microstructures, showed improved performance owing to enhanced mass transport by the thinned electrode, effective utilization of the active sites, and increased Pt utilization. To obtain further performance enhancement, we incorporated a guided gold cracked layer into the MEA with the multiscale patterned membrane. The electrochemically inactive thin gold layer acted as a physical barrier for methanol crossover and the guided cracks provided multiple proton pathways. Our interface engineering utility resulted in an enhancement of the device performance by 42.3% compared with that of the reference.

1. Introduction

The direct methanol fuel cell (DMFC) has received significant attention as an ideal power source that could satisfy the increasing demand for portable electronics owing to its high energy density, environmental friendliness, as well as the ease of handling methanol [1–4]. Nonetheless, to commercialize DMFCs, some obstacles, such as high catalyst loadings and large system volumes, need to be overcome [5,6]. Among DMFC components, the membrane electrode assembly (MEA) is the most important. As a core component of fuel cells, the MEA generates electricity by electrochemical oxidation of methanol and reduction of oxygen at the anode and the cathode, respectively. Since the design of the fuel container and number of stacks are determined by the power and energy generated from the MEA, the fabrication of high-performance MEAs is a key to reducing the volume of DMFCs and the catalyst loading amounts [5].

In DMFCs, performance loss mainly results from two factors: (a) formation of a mixed potential at the cathode due to methanol crossover through an electrolyte membrane [6,7] and (b) slow kinetics of methanol oxidation at the anode [6,8,9]. To resolve the issue of methanol crossover, many approaches have been adopted, such as developing organic/inorganic composite membranes [10,11] and embedding a methanol barrier layer into the membrane surface [12,13]. However, achieving low methanol crossover and high proton conductivity

Abbreviations: DMFC, direct methanol fuel cell; MEA, membrane electrode assembly; PET, polyethylene terephthalate; CCM, catalyst-coated membrane; FE-SEM, field emission scanning electron microscopy; FIB-SEM, focused ion beam-assisted scanning electron microscopy; AFM, atomic force microscopy; EIS, electrochemical impedance spectroscopy; DHE, dynamic hydrogen electrode; RE, reference electrode; CE, counter electrode; WE, working electrode; LSV, linear sweep voltammetry; CO, carbon monoxide; ECSA, electrochemical active surface area; T_g, glass temperature; R_{ct}, charge transfer resistance

* Corresponding author.
** Corresponding author at: School of Chemical and Biological Engineering, Seoul National University, Seoul 08826, Republic of Korea.
*** Corresponding author at: Global Frontier Center for Multiscale Energy Systems, Seoul National University, Seoul 08826, Republic of Korea.
E-mail addresses: yhun00@kangwon.ac.kr (Y.-H. Cho), ysung@snu.ac.kr (Y.-E. Sung), mchoi@snu.ac.kr (M. Choi).
[1] S. Jang and S. Kim contributed equally to this work.

https://doi.org/10.1016/j.nanoen.2017.11.011
Received 16 August 2017; Received in revised form 4 November 2017; Accepted 5 November 2017
Available online 06 November 2017

simultaneously has been challenging owing to methanol permeation resulting from the electro-osmotic drag caused by hydrated protons and diffusion. To resolve other issues, namely low Pt utilization and the slow kinetic behavior of the MEA, many studies have examined the incorporation of a patterned membrane into fuel cell devices using a simple one-dimensional pattern [14,15]. However, an enlarged interfacial area between the anode and the electrolyte membrane results in higher methanol crossover [5], which implies that a trade-off would exist between low methanol crossover and high interfacial area. To solve both these problems simultaneously and thus obtain a high-performance DMFC, we fabricated a MEA with a multiscale patterned membrane and incorporated a guided gold cracked layer into the MEA. Based on the creep-assisted sequential imprinting method [16], we easily fabricated micro-/nano- multiscale hierarchical structures, where the nanopatterns covered the whole surface even on the side surface of microstructures. This enabled fully utilizing the multiscale structural effects. The MEA with the multiscale patterned membrane showed improved performance compared with that of the reference because mass transport was enhanced by the thinned electrode and the effective utilization of catalytic active sites. Moreover, the electrochemically inactive thin gold layer was expected to act as a physical barrier for methanol crossover, with cracks introduced to provide multiple proton pathways. In addition to reduced methanol crossover, the multiscale MEA with guided gold cracked layer achieved an ohmic resistance comparable to that of the reference MEA, and the device performance was significantly enhanced by 42.3% compared with that of the reference.

2. Experimental section

2.1. Fabrication of the prism and nano-patterned polymer molds

The prism array master mold with a 10 μm pitch size (P-10) was prepared through mechanical machining. First, a nickel electroplated stainless steel sample was mechanically machined with a diamond-cutting tool with a specific angle (~45°) [17]. The height of the carved patterns was determined by the cutting depth of the diamond tool. Then, a UV-curable prepolymer resin (PUA MINS 311 RM, Minuta Tech) was poured on the prepared master, and a 300 μm thick polyethylene terephthalate (PET) film was placed onto it as a supporting backbone. After exposed to UV light (Fusion Cure System, Minuta Tech) for about 30 s, the resultant PUA polymer molds were detached from the prism mold. In addition, a polymeric pillar mold with a diameter of 800 nm was fabricated using an 800 nm hole-array-patterned silicon master mold and the same UV curing method. Finally, the polymer molds were subjected to post-surface treatment with octafluorocyclobutane (C_4F_8) gas to reduce the surface energy of the pattern and achieve high chemical stability.

2.2. Preparation of the multiscale prism mold

The multiscale prism mold was fabricated by the creep-assisted sequential imprinting method [16]. First, a Nafion 115 membrane (DuPont) was placed between the as-prepared 800 nm pillar (+)-patterned PUA mold and the glass substrate. Next, this assembly was hot-pressed under constant pressure (~0.8 MPa) at the glass temperature of Nafion (~130 °C) for 10 min. After cooling to ambient temperature, the 800 nm pillar (+)-patterned PUA mold was detached from the Nafion membrane. The resulting 800 nm hole (-)-patterned Nafion membrane was placed between the as-prepared P-10-patterned PUA mold and the glass substrate again. Then, this assembly was hot-pressed at the transition temperature of Nafion (~85 °C) under constant pressure (~4 MPa) for 1 h. Under these conditions, Nafion showed viscoelastic creep behavior. Following the two imprinting processes, the multiscale prism-patterned mold with a 10 μm pitch and an 800 nm pillar (MP-10) was fabricated by casting and UV-curing of PUA resins on top of the sequentially imprinted membrane.

2.3. Preparation of the multiscale patterned membrane and guided metal cracked layer

The Nafion 115 membrane was uniformly placed between the as-prepared PUA mold (P-10 or MP-10) and the glass substrate. Then, the assembly was imprinted under hydraulic pressure (~1.5 MPa) at a temperature of ~130 °C for 10 min. After cooling to room temperature, the patterned Nafion 115 membrane was peeled off the PUA mold. Next, the membrane was cleaned with a 3 wt% hydrogen peroxide solution and reprotonated using a 0.5 M sulfuric acid solution for 1 h at 80 °C. Then, a gold film with a thickness of ~40 nm was deposited on the prepared membrane using a vacuum thermal evaporator (Selcos, South). Next, the membrane with the thin gold film was stretched in the direction perpendicular to the prism using a universal material testing machine (3342 UTM, Instron Corp.) by applying a strain of about 0.25.

2.4. MEA preparation

MEAs with an active area of 5 cm^2 were fabricated by the catalyst-coated membrane (CCM) method. PtRu black (HiSPEC 6000, Johnson Matthey Corp.) and Pt black (HiSPEC 1000, Johnson Matthey Corp.) were used as the anode and cathode catalysts, respectively. Homogeneous catalyst inks were prepared by dispersing each catalyst over Nafion ionomer (5 wt% Nafion solution, DuPont) in an aqueous solution of isopropyl alcohol (IPA, Sigma Aldrich) (volumetric ratio of distiled water:IPA = 10:50), followed by ultrasonic treatment more than 10 min. The prepared catalyst inks were directly sprayed onto the prepared or bare Nafion membranes to fabricate CCMs. The catalyst loadings for the anode and the cathode were fixed at 2.0 mg cm^{-2} and 1.0 mg cm^{-2}, respectively. These CCMs were dried at ~30 °C for more than 12 h. Then, the CCMs were sandwiched between the anode gas diffusion layer (TGP-H-060, Toray) and cathode gas diffusion layer (JNT30-A3, JNTG) without a hot-pressing process.

2.5. Physical characterization

Surface images of various samples used in this study were obtained using field emission scanning electron microscopy (FE-SEM, AURIGA, Carl Zeiss) and cross-sectional images were investigated utilizing focused ion beam-assisted SEM (FIB-SEM, AURIGA, Carl Zeiss), which uses an energy-selective backscattered detector to distinguish each layer more clearly. In addition, the topography of each sample was examined using atomic force microscopy (AFM, NX-10, Park Systems) in noncontact mode with a silicon tip.

2.6. Electrochemical characterization

The prepared MEA was inserted between two graphite plates with a one-channel, serpentine-type flow field. The single cell was assembled by applying torque to each screw of the single cell (~6.4 N m) and then connected to a DMFC station (CNL Energy). Before measuring the DMFC performance of the prepared MEA, the single cell was operated under hydrogen fuel cell conditions. Fully humidified hydrogen and oxygen without back pressure were fed to the anode and the cathode at flow rates of 300 mL min^{-1} and 200 mL min^{-1}, respectively. The temperature of the cell was maintained at 70 °C. The single cell was operated under these conditions until a stabilized cell voltage was achieved at the correspondent discharging current with a scan rate of 36 mA s^{-1}. To estimate the DMFC performance of the prepared MEA, methanol solutions with different concentrations (1.5 M and 3.0 M) were fed to the anode at a flow rate of 1.5 mmol min^{-1}. Nonhumidified air was supplied to the cathode at a flow rate of 200 mL min^{-1}. The single cell polarization curve was measured at a cell temperature of 70 °C by the current sweep method at a scan rate of 18 mA s^{-1}.

Electrochemical impedance spectroscopy (EIS, Zennium, Zahner) was conducted at 0.4 V with an amplitude of 10 mV over the frequency range of 0.1 Hz to 100 kHz to characterize the electrochemical properties of the MEA. EIS was conducted under the same conditions as those for the single cell operation. To demonstrate the effect of membrane patterning on the anode performance, an anode polarization test was performed at 70 °C by supplying fully humidified hydrogen to the cathode at a flow rate of 200 mL min^{-1} instead of non-humidified air. The cathode with hydrogen flowing around it could be considered a dynamic hydrogen electrode (DHE); therefore, anode polarization curves and EIS measurements for the cell were obtained using the cathode as the reference electrode (RE) and the counter electrode (CE) [18] and the anode as the working electrode (WE). To analyze the relative amount of methanol crossover, linear sweep voltammetry (LSV) was conducted at 70 °C by supplying a methanol solution (1.5 M or 3.0 M) and fully humidified nitrogen gas to the anode and the cathode, respectively. Under these conditions, the cathode was used as the WE and the anode was used as the CE. The discharge potential range was 0.00–0.75 V vs. the anode at a scan rate of 2 mV s^{-1}. For the carbon monoxide (CO) stripping experiment, fully humidified hydrogen was fed to the cathode (Pt black electrode), serving as the RE and the CE and CO was fed to the anode (PtRu black electrode). CO was adsorbed at 0.05 V for 10 min. Then, excess CO in the anode was purged out with fully humidified nitrogen for 30 min. The voltammetry was conducted at a cell temperature of 30 °C and the voltage sweep range was 0.05–1.20 V at a scan rate of 20 mV s^{-1}. The electrochemical active surface area (ECSA) was obtained by integration of the adsorbed CO (CO_{ad}) oxidation peak.

3. Results and discussion

3.1. Fabrication of multiscale patterned Nafion membranes

Fig. 1 shows a schematic illustration of the fabrication process for the multiscale prism-patterned Nafion membrane. The multiscale prism mold was fabricated based on the creep-assisted sequential imprinting method [16], which our group has previously developed for constructing multiscale structures. The method consists of successive thermal imprinting processes using thermo-plastic films with varying imprint conditions. In this process, the first imprinting step was performed above the glass temperature (T_g) of the polymer film. When the imprint temperature is higher than the T_g of the polymer, the polymer behaves as a viscous liquid and can easily flow into the openings of the mold [19]. The second imprinting step was then carried out based on the viscoelastic creep behavior of the polymer below the T_g. This creep phenomenon denotes a permanent deformation of the polymer material, even below the T_g, when the material is exposed to long-term mechanical stresses (details are provided in Section 2.2) [16]. Using this creep-assisted sequential imprinting method, we could easily fabricate multiscale hierarchical structures with the advantages of scalability and high throughput. SEM images of the fabricated multiscale prism mold are shown in Fig. S1 and we can easily see that nano-patterns well remained even after the second stamping procedure because

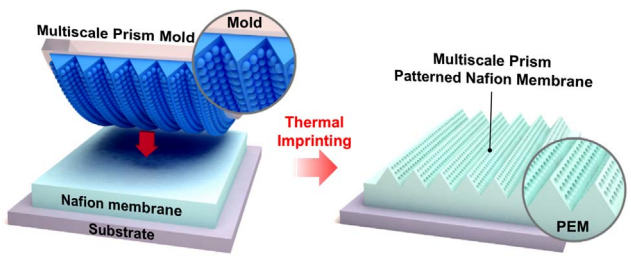

Fig. 1. Schematic for the fabrication of the multiscale prism-patterned membrane by thermal imprinting.

the creep deformation underwent under the Tg of the polymer. This resulted in maximizing the effects of multiscale structures. Next, using the as-prepared P-10 and MP-10 molds, we fabricated patterned Nafion membranes by the thermal imprinting method. Fig. 2a–c shows the SEM images of the pristine, P-10-, and MP-10-patterned Nafion 115 membranes, respectively. Repeated valleys and ridges are clearly seen in both the P10-patterned and MP-10 patterned membranes. In particular, in the MP-10-patterned membrane, additional nano-patterns are carved on the side prism surfaces.

3.2. Enhanced cell performance of DMFCs with multiscale patterned membranes

To evaluate the advantages of the multiscale patterned membrane in DMFCs, pristine, P-10-patterned, and MP-10-patterned membranes were incorporated into MEAs. The patterned side of the membranes was utilized for the anode catalyst layer to improve the reaction kinetics of methanol oxidation in the DMFCs. Commercial PtRu black (atomic ratio of Pt:Ru = 1:1) catalyst was spray-coated onto the patterned side of the membranes. To compare the morphological characteristics of the anode catalyst layers of the three different MEA samples, cross-sectional FIB-assisted SEM images (Fig. 2d–f) were obtained. The catalyst layers were well formed, conforming to the patterned membrane surface. Although the amount of loaded catalyst was the same in all cases, the average thickness varied for each anode catalyst layer: ~8.0 μm for the reference MEA, ~7.2 μm for the P-10 MEA, and ~6.9 μm for the MP-10 MEA. The difference in the anode catalyst layer thickness arose from the enlarged surface area of the patterned membranes, as the catalyst layer thickness was inversely proportional to the surface area of each membrane. The increase in the real surface area was calculated based on the FIB-assisted SEM and AFM images. The surface areas of the P-10-patterned and MP-10-patterned membranes showed increases of ~15% and 27%, respectively relative to that of the flat membrane (Fig. S2 and S3). The further increase of surface area of MP-10-patterned membrane compared to that of the P-10-patterned membrane originated from the nanopatterns which existed on the whole surface of the prism patterns.

Fig. 3a–b shows single cell polarization curves for the MEAs with pristine, P-10-patterned, and MP-10-patterned membranes when fed with methanol solutions with concentrations of 1.5 M and 3.0 M. Both the P-10 and MP-10 MEAs exhibited enhanced performance when compared with the reference MEA under all experimental conditions. The P-10 and MP-10 MEAs showed maximum power densities of 167 (128) mW cm^{-2} and 177 (134) mW cm^{-2}, respectively, in 1.5 (3.0) M methanol solution. The performance enhancement relative to the reference MEA was about 10.5% (15.3%) and 17.2% (20.7%) for the P-10 and MP-10 MEAs, respectively, in 1.5 (3.0) M methanol solution (Table 1). This enhanced performance would be ascribed to both the enlarged membrane–electrode interface contact area and the reduced catalyst layer thickness owing to the use of patterned membranes. The membrane–electrode interface generally contains the greatest number of active sites, where the electrochemical reaction occurs most effectively [20]. Moreover, a thinned anode catalyst layer facilitates mass transport of methanol, resulting in more methanol being easily accessible to the catalytic active sites [14]. Therefore, among the three different MEAs, the MP-10 MEA showed the highest single cell performance owing to the multiscale micro-/nanopatterned membrane. To investigate the effect of the patterned membrane on the overall resistance, EIS was conducted in methanol solutions with concentrations of 1.5 M and 3.0 M. Fig. 3c-d presents EIS spectra (marked points) of tested MEAs together with fitted curves (solid lines) based on the corresponding equivalent circuit (shown in the inset of Fig. 3c), which use the constant phase elements (CPEs) instead of pure capacitors to account for the non-uniform structure of the real condition [21]. The physical meanings of each element employed in the equivalent circuit are as follows [21,22]: (1) L_1 contributes to the inductance of conducting cables and R_m indicates the ohmic resistance of MEA. (2) The

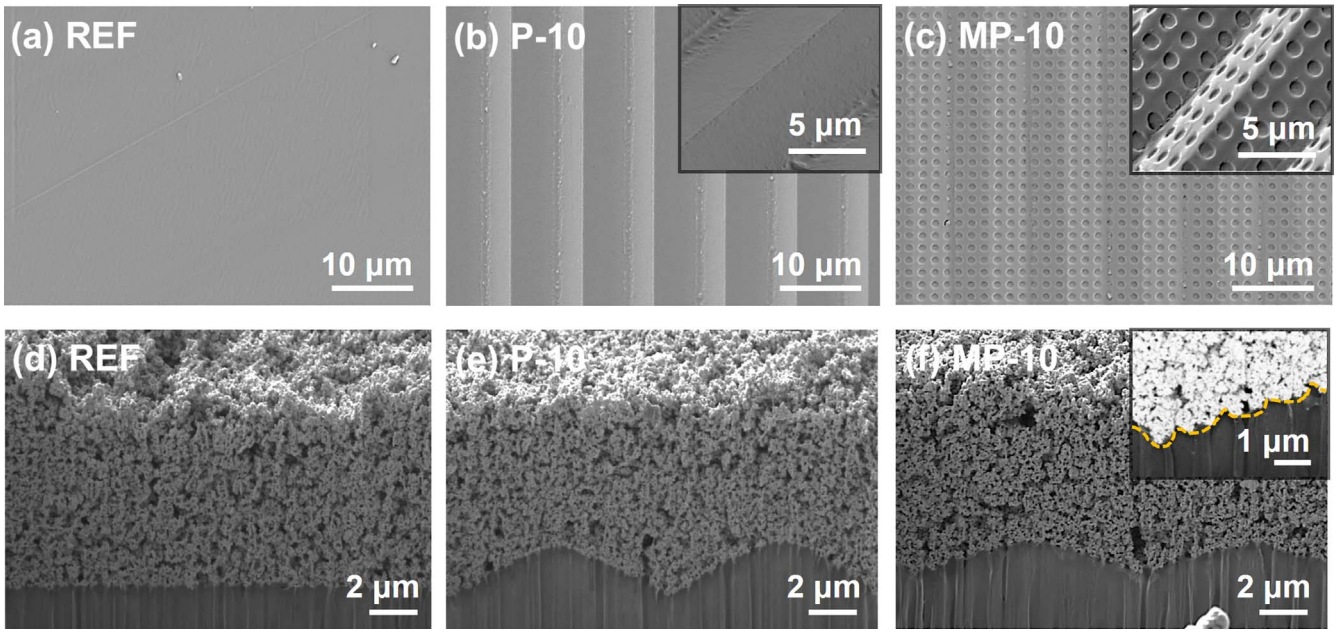

Fig. 2. SEM images of the surfaces of the (a) flat reference, (b) prism-patterned (P-10), and (c) multiscale prism-patterned (MP-10) membranes; FIB-assisted cross-sectional SEM images of the anode catalyst layers of the prepared CCMs with a (d) flat surface, (e) prism pattern (P-10), and (f) multiscale prism pattern (MP-10).

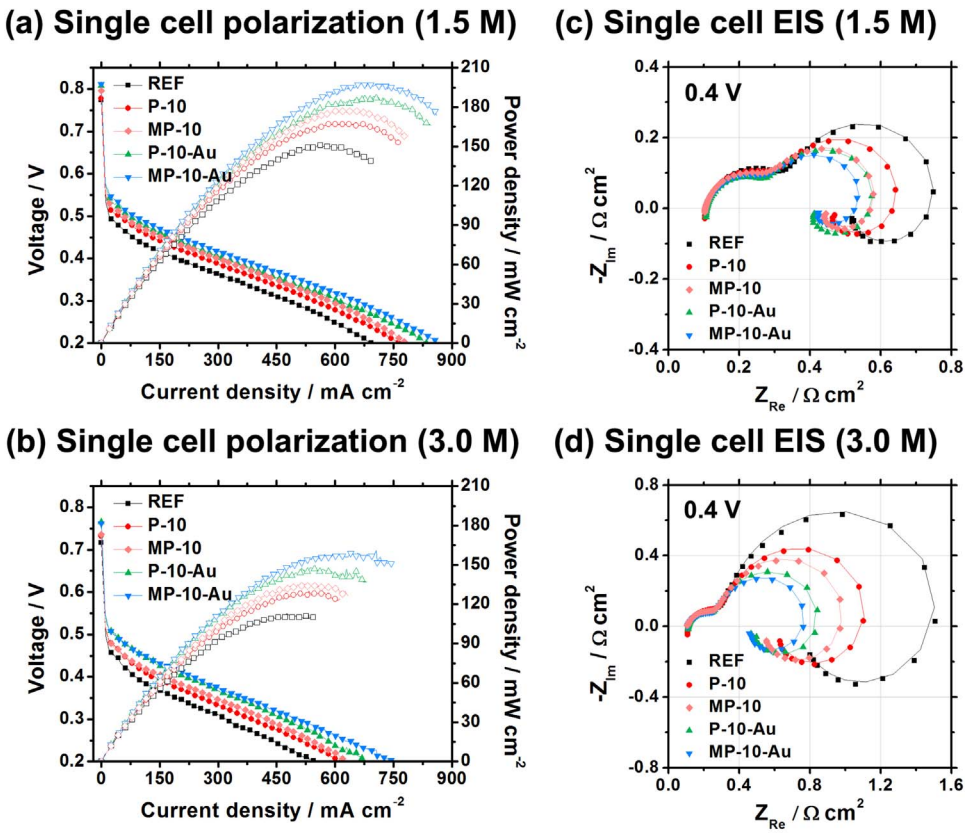

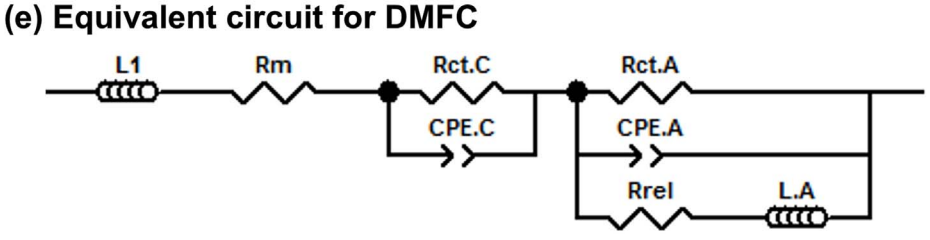

Fig. 3. (a–b) Single cell polarization curves and (c–d) EIS spectra of the reference MEA, MEAs with patterned membranes (P-10 and MP-10), and MEAs with patterned membranes containing a Au layer with guided cracks (P-10-Au and MP-10-Au).

Table 1
Open circuit voltage, current density at 0.4 V, and maximum power density of prepared MEAs at two different methanol concentrations (1.5 M and 3.0 M).

MEA and methanol concentration	Open circuit voltage [V]	Current density at 0.4 V [A cm^{-2}]	Maximum power density [W cm^{-2}]
1.5 M methanol solution			
Reference	0.775	0.193	0.151 (+00.0%)
P-10	0.778	0.262	0.167 (+10.5%)
MP-10	0.796	0.298	0.177 (+17.2%)
P-10-Au	0.808	0.316	0.186 (+23.2%)
MP-10-Au	0.811	0.349	0.197 (+30.5%)
3.0 M methanol solution			
Reference	0.717	0.087	0.111 (+00.0%)
P-10	0.733	0.136	0.128 (+15.3%)
MP-10	0.736	0.158	0.134 (+20.7%)
P-10-Au	0.766	0.215	0.148 (+33.3%)
MP-10-Au	0.762	0.237	0.158 (+42.3%)

Parenthesis (): The increased ratio of the maximum power density compared to the reference MEA.

cathode contribution includes $R_{ct,C}$ and CPE_C indicating the charge transfer resistance and capacitive behavior of the cathode. (3) $R_{ct,A}$ and CPE_A describe the charge transfer resistance of the anode reaction and capacitive behavior of the anode, respectively. L_A and R_{rel} indicate the pseudo-inductance and the relaxation resistance, respectively. The fitted parameters are provided in Table 2. As observed, the ohmic resistance (R_m) of the patterned MEAs is slightly less than that of the reference MEA due to the reduced membrane thickness (~3 μm) compared to the original membrane thickness (~115 μm). The $R_{ct,A}$, which is affected by the methanol oxidation reaction at anode, was related to the semicircle in the EIS spectra at the low frequency ranges. A comparison of the $R_{ct,A}$ values for MEAs with pristine, P-10-patterned and MP-10-patterned membranes showed that the $R_{ct,A}$ values decreased as the surface area of the membrane–electrode interface increased under both 1.5 M and 3.0 M methanol concentrations. The decreased $R_{ct,A}$ of MP-10 MEA compared to the reference MEA was about 72.1% (53.9%) in 1.5 (3.0) M methanol solution. Thus, the reduced $R_{ct,A}$ was responsible for the improved performance of the multiscale patterned MEA.

For better understanding the effect of patterned MEAs on methanol oxidation reaction at anode, anode polarization curves and anode EIS spectra were obtained for the three different MEAs in 3.0 M methanol concentration using the cathode as a DHE by supplying hydrogen instead of air (Fig. 4). The anodic over-potential of the three MEAs at the same current density followed the order: reference > P-10 > MP-10, and the anode R_{ct} decreased as the surface area of the membrane–electrode interface increased. These results showed the same trends as that observed for the single cell polarization curves and EIS spectra. Therefore, we can say that the enlarged surface area of the membrane resulted in enhanced anode performance. In addition, as shown in Fig. S4, the single cell polarization curves of all the MEAs, including the reference MEA, MEAs with patterned membranes (P-10 and MP-10), and MEAs with patterned membranes containing a gold layer with guided cracks (P-10-Au and MP-10-Au), were almost identical when hydrogen was fed to the anode instated of methanol. This result indicates that all the cathodes in the MEAs had the same morphological features because the performance of the MEAs was mainly affected by the oxygen reduction reaction at the cathode under hydrogen/oxygen operating conditions. CO stripping voltammetry were carried out to investigate the effect of the enlarged membrane–electrode interface on the ECSA of the anode catalyst layer (Fig. 5). By using CO adsorption (at about 0.05 V vs. DHE) and CO_{ad} oxidation process (at about 0.5 V vs. DHE) instead of adsorption/desorption of hydrogen, we excluded the effects of the adsorption of –OH species onto the PtRu catalyst that hinder the adsorption of hydrogen (Fig. S5). As displayed in the magnified plots (Fig. 5b), the intensity of the adsorbed CO oxidation peak gradually increased with proportional to the membrane surface area. The ECSA of MP-10 MEA was calculated to be 51.80 $m^2\ g_{PtRu}^{-1}$, which is about 5.5% larger than that of the reference MEA (49.11 $m^2\ g_{PtRu}^{-1}$). Since ECSA reflects the utilization of Pt catalyst, a higher ECSA of the multiscale patterned membrane could account for the enhanced electrocatalytic activity. This enhancement resulted from the enlarged interfacial area between the membrane and the catalyst layer due to the multiscale patterning [14,15,23]. However, the increment in the ECSA (5.5%) was not sufficiently large to completely account for the enhanced performance (17.2%) of the MEA with the multiscale patterned membrane [14,24]. Therefore, to better understand the origin of the performance enhancement, we should consider the comprehensive effects of the MEA with the multiscale patterned membrane, including enhanced mass transport and effective utilization of active sites.

3.3. Further enhanced cell performance of DMFCs with guided metal cracked barriers

To further enhance the performance of the DMFCs by reducing methanol crossover, a thin gold layer with guided cracks was incorporated into the multiscale patterned membrane. The methanol-inactive thin gold layer was expected to act as a physical barrier for methanol crossover and the cracks were expected to provide multiple proton pathways. Fig. 6a shows a schematic illustration of the process for generating a gold layer with guided cracks on the multiscale

Table 2
Fitting parameters for the equivalent circuit model for all the MEAs in different methanol concentrations (1.5 M and 3.0 M, respectively).

	1.5 M methanol solution					**3.0 M methanol solution**				
Parameter	REF	P-10	MP-10	P-10-Au	MP-10-Au	REF	P-10	MP-10	P-10-Au	MP-10-Au
L_1 (x10^{-7}) (H cm^{-2})	2.97	4.97	2.00	4.32	1.53	1.96	8.14	2.82	3.37	0.90
$R_{ct,C}$ (Ohm cm^2)	0.244 (00.0%)	0.231 (−5.3%)	0.211 (−13.5%)	0.192 (−21.3%)	0.191 (−21.7%)	0.221 (00.0%)	0.210 (−5.0%)	0.194 (−12.2%)	0.163 (−26.2%)	0.158 (−28.5%)
CPE_C-T (F cm^{-2})	0.0217	0.0283	0.0292	0.0257	0.0322	0.0409	0.0352	0.0361	0.0286	0.0342
CPE_C-P	0.850	0.845	0.864	0.852	0.856	0.756	0.792	0.801	0.820	0.817
R_m (Ohm cm^2)	0.108	0.103	0.104	0.107	0.106	0.110	0.107	0.106	0.110	0.108
$R_{ct,A}$ (Ohm cm^2)	0.408 (00.0%)	0.347 (−14.9%)	0.294 (−27.9%)	0.321 (−21.2%)	0.288 (−29.4%)	1.402 (00.0%)	0.939 (−33.0%)	0.756 (−46.1%)	0.682] (−51.4%)	0.634 (−54.8%)
CPE_A-T (F cm^{-2})	0.137	0.156	0.156	0.190	0.202	0.127	0.142	0.142	0.155	0.195
CPE_A-P	1.062	1.028	1.037	0.994	0.978	0.975	0.978	1.008	0.960	0.935
R_{rel} (Ohm cm^2)	0.244	0.212	0.227	0.169	0.220	0.607	0.429	0.340	0.263	0.259
L_A (H cm^{-2})	0.133	0.0798	0.0784	0.0637	0.0623	0.569	0.308	0.278	0.143	0.140

Parenthesis (): The reduction ratio of the charge transfer resistance compared to the reference MEA.

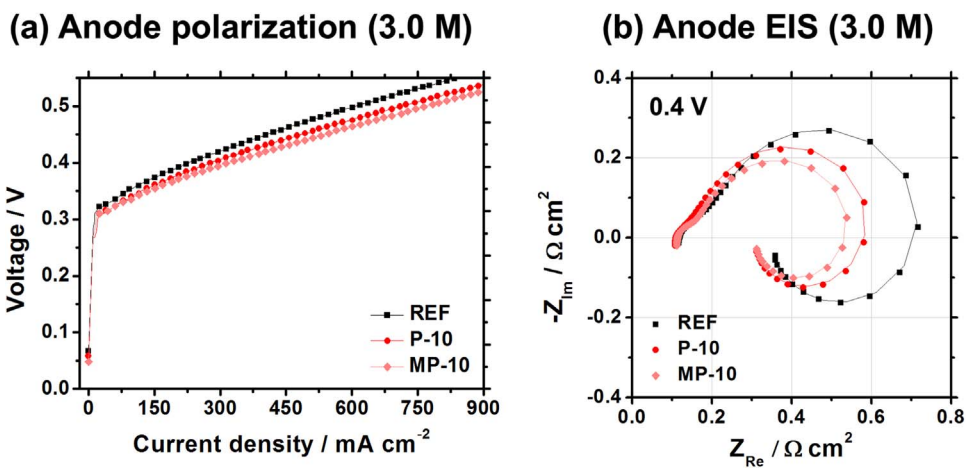

Fig. 4. (a) Anode polarization curves and (b) anode EIS spectra of the reference MEA and MEAs with prism- (P-10) and multiscale prism-patterned (MP-10) membranes.

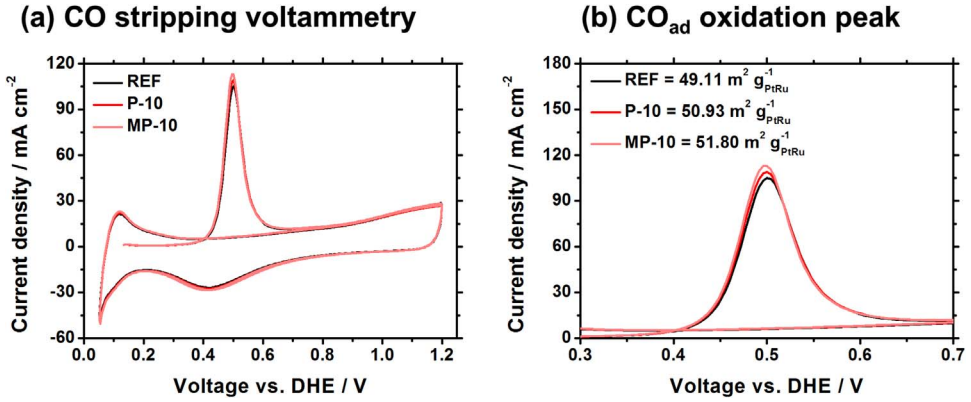

Fig. 5. CO stripping voltammograms of the anode catalyst layers of the reference MEA and MEAs with prism- (P-10) and multiscale prism-patterned (MP-10) membranes.

patterned membrane. The thin gold layer (~40 nm) was deposited onto the patterned membrane surface (P-10 and MP-10) using a thermal evaporator. Then, the gold deposited patterned membrane was stretched with a strain of ~0.25 in the direction perpendicular to the prism pattern. After the stretching process, cracks were well formed, especially in the valleys of the prism pattern, owing to elastic modulus mismatch and confinement of the stresses in the valleys of the prism pattern [25–27]. Fig. 6b shows the SEM images of the surface

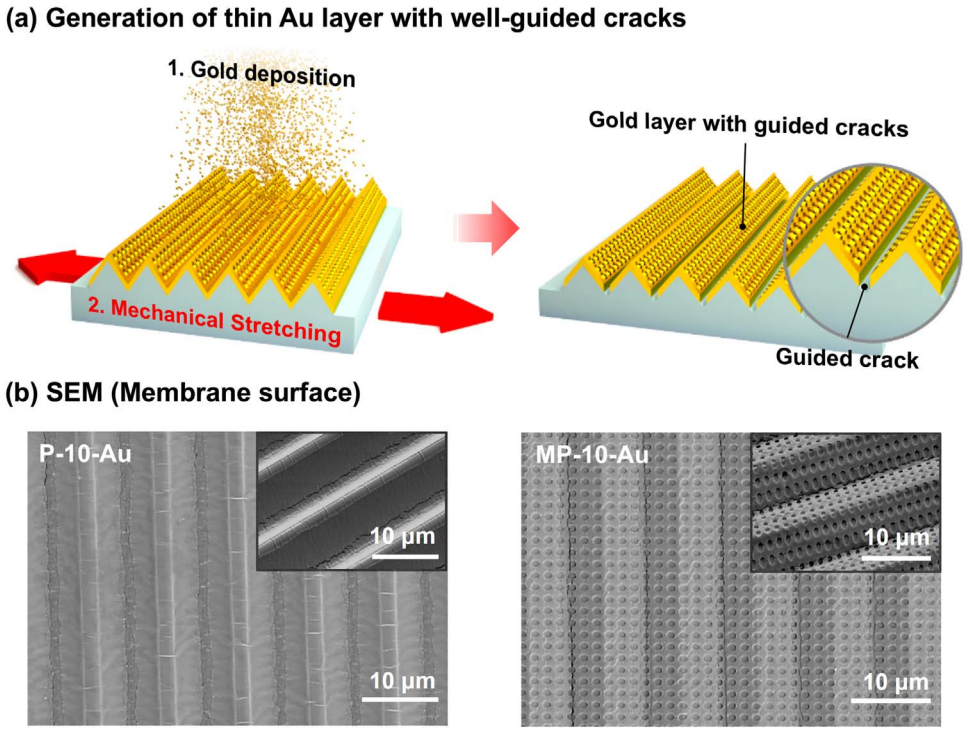

Fig. 6. (a) Schematic for generating guided Au cracks by simple mechanical stretching (strain of ~0.25) and (b) SEM images of the surfaces of prism-patterned (P-10-Au) and multiscale prism-patterned (MP-10-Au) membranes with guided Au cracks.

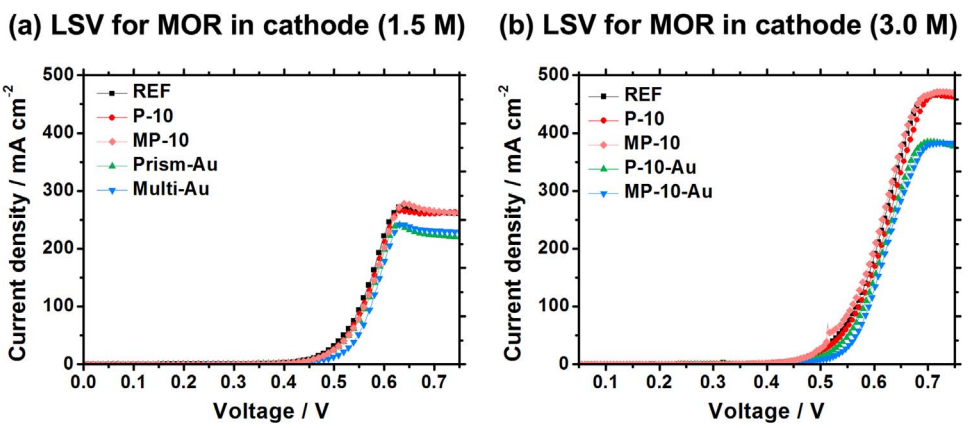

Fig. 7. Limiting current density measurements for the reference MEA, MEAs with patterned membranes (P-10 and MP-10), and MEAs with patterned membranes and a guided Au cracked layer (P-10-Au and MP-10-Au).

morphologies of the gold deposited patterned membranes with guided cracks (P-10-Au and MP-10-Au). The images show that the cracks are well controlled parallel to the prism direction in both cases, with widths of under 100 nm. By using the stress-concentrated morphology of the patterned membrane, we can control and design the generation of cracks. These controllable cracks have several advantages over randomly formed cracks, as (1) the same crack morphology can be reproduced easily, and (2) parametric studies on the effect of crack gap size and areal fraction of the cracks are possible. To confirm the effect of the gold layer with guided cracks on methanol permeation in the cathode, we measured the limiting current densities from the LSV curves for methanol oxidation at the cathode [28]. As seen in Fig. 7a–b, both the P-10-Au and MP-10-Au MEAs containing gold layers with guided cracks showed lower limiting current densities than the reference MEA and the patterned MEAs without the gold layers. The limiting current densities of the MEAs with the patterned membranes were slightly higher owing to the enlarged membrane–electrode interface and thinned anode catalyst layer [5]. These results show that while the MEAs with patterned membranes did not reduce the methanol crossover rate, the incorporation of gold layer with guided cracks has a critical effect on reducing methanol crossover.

The single cell polarization curves for the MEAs with guided gold cracked layers were also presented in Fig. 3a-b, when fed with 1.5 M and 3.0 M methanol solutions (Table 1). In the polarization curves, both P-10-Au and MP-10-Au MEAs with guided gold cracked layers exhibited significantly enhanced performance compared with the reference MEA and patterned MEAs without gold layers. The P-10-Au and MP-10-Au MEAs with guided gold cracked layers showed maximum power densities of 186 mW cm^{-2} (148 mW cm^{-2}) and 197 mW cm^{-2} (158 mW cm^{-2}) in 1.5 M (3.0 M) methanol concentrations, denoting performance enhancements of about 23.2% (33.3%) and 30.5% (42.3%) compared to that of the reference MEA, respectively. EIS measurements for the MEAs guided gold cracked layers were conducted to figure out the effect of guided gold cracked layer (Fig. 3c–d). The charge transfer resistance of cathode ($R_{ct,C}$), which is affected by the cathode reaction, was related to the semicircle in the EIS spectra at the high frequency ranges. The fitted parameters are provided in Table 2. A comparison of the spectra for all the samples shows that the MEAs with guided gold cracked layers have much lower $R_{ct,C}$ values than that of the reference MEA while maintaining a comparable ohmic resistance. The decreased $R_{ct,C}$ values of the MEAs with guided gold cracked layers decreased about 78.7% (73.8%) and 78.3% (71.5%) for the P-10-Au and MP-10-Au MEAs in 1.5 (3.0) M methanol concentration. This result could be attributed to the decreased mixed potential at cathode resulting from the low methanol crossover, which implies that the effect of the guided gold cracked barrier is more prominent at higher methanol concentrations. Considering the reduction ratio of $R_{ct,C}$ compared to the reference MEA, the patterned MEAs without guided gold cracked layers increased as the methanol concentration increases from 1.5M to 3.0 M, the further decreased $R_{ct,C}$ at higher methanol concentration is another indication of reduced methanol crossover when applying the thin gold-based membranes. Notably, the incorporation of guided gold cracked layers into the MEAs does not affect the Pt utilization and the number of available active sites (Fig. S6). Therefore, further performance enhancements of the MEAs with patterned membranes were successfully achieved by incorporating a gold layer with guided cracks, which can be attributed to two factors. First, the multiscale patterned membrane can significantly increase the interfacial area between the membrane and the catalyst layer. Therefore, in the MEA, we can effectively utilize the enlarged interfacial area, where electrochemical reactions are the most effective. Moreover, a thinned catalyst layer increases mass transport of the fuel, resulting in more methanol being easily accessible to the catalytic active sites. Second, the gold layer with guided cracks plays a significant role in reducing the methanol crossover rate while maintaining a comparable proton transport ability because of the multiple cracks. Therefore, among the five different MEAs, the MP-10-Au MEA showed the highest cell performance owing to a synergistic effect between the enlarged membrane–electrode interface of the patterned membrane and the reduced methanol crossover rate of the gold layer with guided cracks. These effects are briefly summarized in Fig. 8. Surprisingly, the device performance of the MP-10-Au MEA with a guided gold cracked layer was similar to that of the reference MEA operated in the presence of O_2 instead of air (Fig. S7). Considering the thermodynamic potential of a DMFC, which can be calculated using the Nernst equation [29],

$$V_{DMFC,\,thermo} = E_0 + \frac{RT}{6F}\ln\left\{\frac{a_{CH_3OH} * (a_{O_2})^{1.5}}{a_{CO_2} * (a_{H_2O})^2}\right\}$$

where E_0 is the standard potential, R is the gas constant, F is the Faraday's constant, and a_{CH_3OH}, a_{O_2}, a_{CO_2}, and a_{H_2O} are the chemical activity of methanol, oxygen, carbon dioxide, and water, respectively, the thermodynamic potential should be lower for the MP-10-Au MEA in air feeding conditions (a_{O_2} ~0.21) than for the reference MEA in O_2 feeding conditions (a_{O_2} ~1). Therefore, the comparable performances

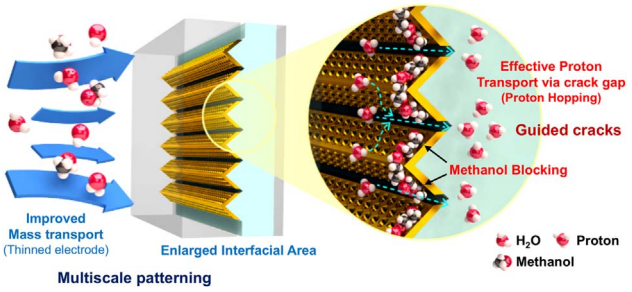

Fig. 8. Schematic illustration of the effects of the enlarged interfacial area and the guided Au cracked barrier.

of the MP-10-Au MEA under air and the reference MEA under O_2 indicate that an interface-engineered MEA with a multiscale patterned membrane and guided gold cracked layer can significantly improve DMFC performance. Furthermore, to confirm the effectiveness of a guided gold cracked layer in terms of proton conductivity and methanol crossover, single cell polarization curves and EIS spectra for randomly cracked gold layer (S ~0.25) and non-cracked gold layer were measured. The MEA with non-cracked gold layer shows reduced performance about 41.1% and increased ohmic resistance about 70.2% than those of reference (Fig. S8). This result indicates that the non-cracked gold layer works as a good methanol barrier, but it also prevents proton bonded with water molecules to permeate through the electrolyte membrane due to the absence of proton pathways. Interestingly, the MEA with the randomly cracked gold layer shows higher performance (164 mW cm^{-2}) than that of reference (151 mW cm^{-2}) but still exhibits lower performance and larger ohmic resistance than those of MEAs with guided gold cracked layer. When same stress applied to the gold coated-flat membrane (strain ~ 0.25), the stress was widely distributed on the surface of gold coated-flat membrane, and the cracks were not fully formed on the whole surface of the gold layer. However, in the case of the P-10-Au and MP-10-Au MEAs, the well-ordered cracks could be formed over the entire surface owing to the existence of the valleys of prism, where the stress could be concentrated. The difference is clearly confirmed by comparing the morphological surface features (Fig. 6b and Fig. S9).

To address the cost issue and evaluate the economic impact of incorporation of gold cracked layer into the MEA, the amount of gold used in our systems was calculated. The thickness of gold layer is about ~ 40 nm (~0.0772 mg cm^{-2}) and the amount of gold is about ~3.32% of the amount of platinum catalyst (2.33 mg cm^{-2}) used in this system, even excluding the amount of ruthenium (0.67 mg cm^{-2}). Considering the improved performance of MP-10-Au MEA about ~33.3% (42.3%) relative to that of the reference MEA in 1.5 M (3.0 M) methanol condition and that the fuel cell system is comprised of many components, the marginally increased noble metal in MEA (~3.32%) is a very slight cost. However, to achieve the both high performance and economic competitiveness of MEA, it is encouraged to find more cheap materials with electrochemically stable and applicable for our systems. Among the materials that can be deposited by evaporator system, silicon dioxide and silver could be good candidates. Silicon dioxide is a very cheap, abundant, and electrochemically inactive oxide material. When it comes to silver, the price of silver (~$16.68 toz^{-1}) is much cheaper than gold (~$1279.32 toz^{-1}) or platinum (~$915.00 toz^{-1}) [30] and has much higher standard reduction potential (0.799 V) than that of the proton. Therefore, silicon dioxide and silver layers could be suitable alternatives to replace gold layer and we successfully generated guided cracked layer using thin silver film (~40 nm). (Fig. S10)

4. Conclusions

We report herein a high-performance DMFC based on interface engineering between the membrane and the catalyst layer by using multiscale patterned membrane and guided metal cracked layer. The multiscale patterned membrane enhanced performance by improving mass transport, active site utilization, and Pt utilization. Based on this multiscale patterned membrane, we additionally incorporated a guided gold cracked layer. This guided thin gold cracked layer effectively reduced the methanol crossover rate while maintaining the proton transport ability owing to the existence of multiple cracks. The MEA with the multiscale patterned membrane and a guided gold cracked layer showed a performance improvement of over 42.3% relative to that of the reference MEA with a flat membrane. The effects of crack gap size and areal fraction of the cracks on reducing methanol crossover and maintaining proton conductivity, as well as the other cheaper materials that can be replaced to the gold layer such as silver and silicon dioxide, which studies are currently under investigation. We believe that the interface engineering reported in this study provides a practical and feasible route to fabricate high-performance fuel cells and holds a potential for application to other energy devices.

Acknowledgements

This work was supported by the Global Frontier R&D Program of the Center for Multiscale Energy Systems, funded by the National Research Foundation under the Ministry of Education, Science and Technology, Korea (2012M3A6A7054855); the Institute for Basic Science (IBS) in Korea (IBS-R006-D1); and the Basic Science Research Program (2016R1D1A3B03934752, 2016R1C1B1014564), through the National Research Foundation of Korea (NRF), which is funded by the Ministry of Education.

Appendix A. Supporting information

Supplementary data associated with this article can be found in the online version at http://dx.doi.org/10.1016/j.nanoen.2017.11.011.

References

[1] S.K. Kamarudin, F. Achmad, W.R.W. Daud, Overview on the application of direct methanol fuel cell (DMFC) for portable electronic devices, Int. J. Hydrog. Energy 34 (2009) 6902–6916.
[2] T. Zhao, C. Xu, R. Chen, W. Yang, Mass transport phenomena in direct methanol fuel cells, Prog. Energy Combust. Sci. 35 (2009) 275–292.
[3] J.N. Tiwari, R.N. Tiwari, G. Singh, K.S. Kim, Recent progress in the development of anode and cathode catalysts for direct methanol fuel cells, Nano Energy 2 (2013) 553–578.
[4] J. Xie, Q. Zhang, L. Gu, S. Xu, P. Wang, J. Liu, Y. Ding, Y.F. Yao, C. Nan, M. Zhao, Ruthenium–platinum core–shell nanocatalysts with substantially enhanced activity and durability towards methanol oxidation, Nano Energy 21 (2016) 247–257.
[5] H.-T. Kim, T.V. Reshentenko, H.-J. Kweon, Microstructured membrane electrode assembly for direct methanol fuel cell, J. Electrochem. Soc. 154 (2007) B1034–B1040.
[6] A. Omosebi, R.S. Besser, Electron beam patterned Nafion membranes for DMFC applications, J. Power Sources 228 (2013) 151–158.
[7] D. Sebastian, A. Serov, I. Matanovic, K. Artyushkova, P. Atanassov, A. Arico, V. Baglio, Insights on the extraordinary tolerance to alcohols of Fe-NC cathode catalysts in highly performing direct alcohol fuel cells, Nano Energy 34 (2017) 195–204.
[8] M. Ahmed, I. Dincer, A review on methanol crossover in direct methanol fuel cells: challenges and achievements, Int. J. Energy Res. 35 (2011) 1213–1228.
[9] S. Wu, J. Liu, D. Liang, H. Sun, Y. Ye, Z. Tian, C. Liang, Photo-excited in situ loading of Pt clusters onto rGO immobilized SnO 2 with excellent catalytic performance toward methanol oxidation, Nano Energy 26 (2016) 699–707.
[10] C.-Y. Yen, C.-H. Lee, Y.-F. Lin, H.-L. Lin, Y.-H. Hsiao, S.-H. Liao, C.-Y. Chuang, C.-C.M. Ma, Sol–gel derived sulfonated-silica/Nafion® composite membrane for direct methanol fuel cell, J. Power Sources 173 (2007) 36–44.
[11] D. Jung, S. Cho, D. Peck, D. Shin, J. Kim, Preparation and performance of a Nafion®/montmorillonite nanocomposite membrane for direct methanol fuel cell, J. Power Sources 118 (2003) 205–211.
[12] A. Casalegno, F. Bresciani, V. Di Noto, C. Casari, A.L. Bassi, E. Negro, R. Marchesi, F. Di Fonzo, Nanostructured Pd barrier for low methanol crossover DMFC, Int. J. Hydrog. Energy 39 (2014) 2801–2811.
[13] S. Yoon, G. Hwang, W. Cho, I.-H. Oh, S.-A. Hong, H. Ha, Modification of polymer electrolyte membranes for DMFCs using Pd films formed by sputtering, J. Power Sources 106 (2002) 215–223.
[14] L. Pu, J. Jiang, T. Yuan, J. Chai, H. Zhang, Z. Zou, X.-M. Li, H. Yang, Performance improvement of passive direct methanol fuel cells with surface-patterned Nafion® membranes, Appl. Surf. Sci. 327 (2015) 205–212.
[15] Y.-H. Cho, J.W. Bae, O.-H. Kim, J.Y. Jho, N. Jung, K. Shin, H. Choi, H. Choe, Y.-H. Cho, Y.-E. Sung, High performance direct methanol fuel cells with micro/nano-patterned polymer electrolyte membrane, J. Membr. Sci. 467 (2014) 36–40.
[16] S. Jang, M. Kim, Y.S. Kang, Y.W. Choi, S.M. Kim, Y.-E. Sung, M. Choi, Facile multiscale patterning by creep-assisted sequential imprinting and fuel cell application, ACS Appl. Mater. Interfaces 8 (2016) 11459–11465.
[17] S.M. Kim, Y.S. Kang, C. Ahn, S. Jang, M. Kim, Y.-E. Sung, S.J. Yoo, M. Choi, Prism-patterned Nafion membrane for enhanced water transport in polymer electrolyte membrane fuel cell, J. Power Sources 317 (2016) 19–24.
[18] J.T. Müller, P.M. Urban, W.F. Hölderich, Impedance studies on direct methanol fuel cell anodes, J. Power Sources 84 (1999) 157–160.
[19] S.Y. Chou, P.R. Krauss, P.J. Renstrom, Imprint lithography with 25-nanometer resolution, Science 272 (1996) 85–87.
[20] M. Aizawa, H. Gyoten, A. Salah, X. Liu, Pillar structured membranes for suppressing cathodic concentration overvoltage in PEMFCs at elevated temperature/low relative humidity, J. Electrochem. Soc. 157 (2010) B1844–B1851.
[21] Q. Cheng, Y. Wang, J. Jiang, Z. Zou, Y. Zhou, J. Fang, H. Yang, Shape-controlled

porous heterogeneous PtRu/C/Nafion microspheres enabling high performance direct methanol fuel cells, J. Mater. Chem. A 3 (2015) 15177–15183.
[22] T. Yuan, L. Pu, Q. Huang, H. Zhang, X. Li, H. Yang, An effective methanol-blocking membrane modified with graphene oxide nanosheets for passive direct methanol fuel cells, Electrochim. Acta 117 (2014) 393–397.
[23] Y. Jeon, D.J. Kim, J.K. Koh, Y. Ji, J.H. Kim, Y.-G. Shul, Interface-designed membranes with shape-controlled patterns for high-performance polymer electrolyte membrane fuel cells, Sci. Rep. 5 (2015) 16394.
[24] J.W. Bae, Y.-H. Cho, Y.-E. Sung, K. Shin, J.Y. Jho, Performance enhancement of polymer electrolyte membrane fuel cell by employing line-patterned Nafion membrane, J. Ind. Eng. Chem. Res. 18 (2012) 876–879.
[25] D. Kang, P.V. Pikhitsa, Y.W. Choi, C. Lee, S.S. Shin, L. Piao, B. Park, K.-Y. Suh, T.-I. Kim, M. Choi, Ultrasensitive mechanical crack-based sensor inspired by the spider sensory system, Nature 516 (2014) 222–226.
[26] S.M. Kim, C.-Y. Ahn, Y.-H. Cho, S. Kim, W. Hwang, S. Jang, S. Shin, G. Lee, Y.-E. Sung, M. Choi, High-performance fuel cell with stretched catalyst-coated membrane: one-step formation of cracked electrode, Sci. Rep. 6 (2016) 26503.
[27] B.C. Kim, T. Matsuoka, C. Moraes, J. Huang, M. Thouless, S. Takayama, Guided fracture of films on soft substrates to create micro/nano-feature arrays with controlled periodicity, Sci. Rep. 3 (2013) 3027.
[28] J. Prabhuram, T. Zhao, H. Yang, Methanol adsorbates on the DMFC cathode and their effect on the cell performance, J. Electroanal. Chem. 578 (2005) 105–112.
[29] R.F. Mann, J.C. Amphlett, M.A. Hooper, H.M. Jensen, B.A. Peppley, P.R. Roberge, Development and application of a generalised steady-state electrochemical model for a PEM fuel cell, J. Power Sources 86 (2000) 173–180.
[30] K. Lee, H. Choi, D.S. Kim, M.S. Jang, M. Choi, Vertical stacking of three-dimensional nanostructures via an aerosol lithography for advanced optical applications, Nanotechnology (2017).

Segeun Jang received his B.S. degree in mechanical engineering from Yonsei University in 2013, and he is currently a Ph.D. candidate in the School of Mechanical and Aerospace Engineering at Seoul National University under the supervision of Prof. Mansoo Choi. His research has been focused on novel ways to fabricate multiscale and multifunctional structures for energy devices, including perovskite solar cells and polymer electrolyte membrane fuel cells.

Sungjun Kim received his B.S. degree from the School of Chemical and Biological Engineering at Seoul National University in 2015, and he is currently a Ph.D. student in the School of Chemical and Biological Engineering at Seoul National University under the supervision of Prof. Yung-Eun Sung. His research has been focused on electrochemical energy conversion and storage materials and devices.

Sang Moon Kim received his Ph.D. degree from the School of Mechanical and Aerospace Engineering at Seoul National University in 2015, and he began his independent career in 2016 as an assistant professor in the Department of Mechanical Engineering at Incheon National University. His research interests are focused on multiscale design and fabrication of polymeric architectures for wettability control and fuel cell applications.

Jiwoo Choi received his B.S. degree in mechanical engineering from Seoul National University in 2016, and he is currently a Ph.D. student in the School of Mechanical and Aerospace Engineering at Seoul National University. He has been working on fabrication of multiscale and multifunctional structures and their application in energy devices, especially polymer electrolyte membrane fuel cells.

Jehyeon Yeon received his B.S. degree in mechanical engineering from Seoul National University in 2016, and he is currently a Ph.D. student in the School of Mechanical and Aerospace Engineering at Seoul National University. His research has been focused on carbon nanoparticles synthesized using laser pyrolysis and their application as catalyst supports in energy devices, including polymer electrolyte membrane fuel cells.

Kijoon Bang earned his B.S. degree in physics from Yonsei University in 2016, and he is currently pursuing his Ph.D. in multiscale mechanical engineering at Seoul National University. His graduate studies have focused on the fabrication of perovskite solar cells along with semi-empirically computing device physics.

Chi-Yeong Ahn received his B.S. degree from the School of Chemical Engineering at the University of Ulsan in 2011, and he is currently a Ph.D. student in the School of Chemical and Biological Engineering at Seoul National University under the supervision of Prof. Yung-Eun Sung. His research has been focused on electrochemical energy conversion and storage materials and devices.

Wonchan Hwang received his B.S. degree in chemical and biochemical engineering from Dongguk University in 2015, and he is currently a Ph.D. student in the School of Chemical and Biological Engineering at Seoul National University under the supervision of Prof. Yung-Eun Sung. His research interests include electrochemical energy conversion and storage devices.

Min Her received his B.S. degree from the School of Chemical and Biological Engineering at Seoul National University in 2017, and he is currently a Ph.D. student in the School of Chemical and Biological Engineering at Seoul National University under the supervision of Prof. Yung-Eun Sung. His research has been focused on electrochemical energy conversion and storage materials and devices.

Yong-Hun Cho has been an assistant professor in the Department of Chemical Engineering at Kangwon National University in South Korea since 2015. He received his Ph.D. degree from the School of Chemical and Biological Engineering at Seoul National University in 2009. His research has been focused on electrode structures in fuel cells and lithium ion batteries.

Yung-Eun Sung received his Ph.D. degree in chemistry from the University of Illinois at Urbana-Champaign, USA. He completed postdoctoral studies in Prof. Allen Bard's laboratory at the University of Texas at Austin. He started as an Assistant Professor at Gwangju Institute of Science and Technology in 1998. He moved to Seoul National University in 2004 and became a professor of chemical and biological engineering in 2008. He also started as a group leader at the Center for Nanoparticle Research, Institute of Basic Science (IBS) in 2012. His research interests include electrochemical energy conversion and storage devices.

Mansoo Choi has been a professor in the Department of Mechanical and Aerospace Engineering at Seoul National University in South Korea since 1991. He obtained his Ph.D. degree in 1987 from the University of California, Berkeley. He is currently the president of the International Aerosol Research Assembly (IARA), the editor-in-chief of the Journal of Aerosol Science, and the director of the Global Frontier Center for Multiscale Energy Systems. His research centers on the fabrication of multiscale energy devices via ion-assisted aerosol lithography and the aerosol-based synthesis of novel nanomaterials.